BCL6 inhibition ameliorates resistance to ruxolitinib in *CRLF2*-rearranged acute lymphoblastic leukemia

Shinobu Tsuzuki,[1] Takahiko Yasuda,[2] Hiroaki Goto,[3] Naoko Maeda,[4] Koshi Akahane,[5] Takeshi Inukai,[5] Hideyuki Yamamoto,[6] Sivasundaram Karnan,[1] Akinobu Ota,[1] Toshinori Hyodo,[1] Hiroyuki Konishi,[1] Yoshitaka Hosokawa,[1] Hitoshi Kiyoi[7] and Fumihiko Hayakawa[8]

[1]Department of Biochemistry, Aichi Medical University, School of Medicine, Nagakute, Aichi; [2]Clinical Research Center, National Hospital Organization Nagoya Medical Center, Nagoya, Aichi; [3]Division of Hematology/Oncology, Kanagawa Children's Medical Center, Yokohama, Kanagawa; [4]Department of Pediatrics, National Hospital Organization Nagoya Medical Center, Nagoya, Aichi; [5]Department of Pediatrics, Graduate School of Medicine, University of Yamanashi, Chuo, Yamanashi; [6]Department of Hematology, Fujita Health University School of Medicine, Toyoake, Aichi; [7]Department of Hematology and Oncology, Nagoya University Graduate School of Medicine, Nagoya, Aichi and [8]Department of Integrated Health Sciences, Division of Cellular and Genetic Sciences, Nagoya University Graduate School of Medicine, Nagoya, Aichi, Japan

Correspondence: S. Tsuzuki
tsuzukis@aichi-med-u.ac.jp

Received: February 17, 2022.
Accepted: August 12, 2022.
Prepublished: August 25, 2022.

https://doi.org/10.3324/haematol.2022.280879

Supplementary Table S1 A list of materials used in this study

antibodies for flow cytometry	product number	supplier	clone	isotype
APC anti-human TSLPR(CRLF2)	322807	Biolegend	1B4	mouse IgG1,k
APC anti-human CD45	304011	Biolegend	HI30	mouse IgG1,k
APC anti-human CD262(TNFRS10B)	307407	Biolegend	DJR2-4(7-8)	mouse IgG1,k
PE anti-human CD95(FAS)	305607	Biolegend	DX2	mouse IgG1,k
PE anti-human CD19	302208	Biolegend	HIB19	mouse IgG1,k
PE Mouse IgG1,k Isotyoe Ctrl	981802	Biolegend	MOPC-21	mouse IgG1,k
APC Mouse IgG1,k Isotyoe Ctrl	981806	Biolegend	MOPC-21	mouse IgG1,k

antibodies for western blot	product number	supplier	clone	
BAD	9239	Cell Signaling Technology	D24A9	Rabbit mAb
BAK	6947	Cell Signaling Technology	D2D3	Rabbit mAb
BAX	5023	Cell Signaling Technology	D2E11	Rabbit mAb
BCL2	2870	Cell Signaling Technology	50E3	Rabbit mAb
BCL6	14895	Cell Signaling Technology	D412V	Rabbit mAb
BCLxL	2764	Cell Signaling Technology	54H6	Rabbit mAb
BID	2002	Cell Signaling Technology		Rabbit polyclonal
BIM	2933	Cell Signaling Technology	C34C5	Rabbit mAb
GAPDH	5174	Cell Signaling Technology	D16H11	Rabbit mAb
MCL1	5453	Cell Signaling Technology	D35A5	Rabbit mAb
NOXA	sc-56169	Santa Cruz Biotechnoligy	114C307	Mouse mAb
p21 Waf1/Cip1	2947	Cell Signaling Technology	12D1	Rabbit mAb
TP53	sc-126	Santa Cruz Biotechnoligy	DO-1	Mouse mAb
Phospho-STAT5 (Tyr694)	4322	Cell Signaling Technology	D47E7	Rabbit mAb
PUMA	4976	Cell Signaling Technology		Rabbit polyclonal
STAT5	9363	Cell Signaling Technology		Rabbit polyclonal
SURVIVINE	sc-17779	Santa Cruz Biotechnoligy	D-8	Mouse mAb
XIAP	2045	Cell Signaling Technology	3B6	Rabbit mAb
MYC	sc-764	Santa Cruz Biotechnoligy		Rabbit polyclonal

drugs	product number	supplier	targets of inhibition
Ruxolitinib	HY-50856	MedChemExpress	JAK1/2
FX1	S8591	Selleck	BCL6
BI3802	S6937	Selleck	BCL6
BI3812	S8735	Selleck	BCL6
Pifithrin-α	S2929	Selleck	TP53
CHZ868	HY-18960	MedChemExpress	JAK2
venetoclax	S8048	Selleck	BCL-2
SH-4-54	S7337	Selleck	STAT3, STAT5
STAT-5-IN-1	S6784	Selleck	STAT5
S63845	S8383	Selleck	MCL1
A-1155463	S7800	Selleck	BCLxL
NVP-CGM097	S7875	Selleck	MDM2
MI-773	S7649	Selleck	MDM2
busulfan	B2635	Sigma-Aldrich	preconditioning of mice
enrofloxacin	Baytril 10%	BAYER Pharmaceuticals	antibiotics for mice

cells	product number	supplier
MHH-CALL-4	ACC 337	DSMZ
MUTZ-5	ACC 490	DSMZ
NAGL-1	IFO50479	JCRB
Reh	CRL-8286	ATCC
NALM-1	CRL-1567	ATCC
Kasumi-2	JCRB1395	JCRB
Kasumi-7	JCRB1401	JCRB
NALM6	CRL-3273	ATCC
YCUB5	-	Hiroaki Goto
KOPN49	-	Koshi Akahane, Takeshi Inukai

Supplementary Table S1 (cont'd from the previous page)

others	product number	supplier
SuperKillerTRAIL	AG-40T-0002-C020	AdipoGen
Anti-Fas(CD95) clone CH-11	SY-001	MBL
Annexin V-FITC	4700-100	MBL
JC-1	MT09	Dojindo

primers	
BCL6 qPCR	5'-AGAGCCCATAAAACGGTCCT-3'
	5'-TCCCTCAGGGTTGATCTCAG-3'
GAPDH qPCR	5'-CTGACTTCAACAGCGACACC-3'
	5'-TAGCCAAATTCGTTGTCATACC-3'

shRNA target sequence		
BCL6_1	CCCATGATGTAGTGCCTCTTT	(Ref: Nat. Immunol. 14(10);1084, 2013)
BCL6_2	CCACAGTGACAAACCCTACAA	(Ref: Nat. Immunol. 14(10);1084, 2013)
MYC_1	CAGTTGAAACACAAACTTGAA	(Sigma: TRCN0000039640)
MYC_2	CCTGAGACAGATCAGCAACAA	(Sigma: TRCN0000039642)
Luciferase	CTTACGCTGAGTACTTCGA	(Ref: Blood 117(14):3858, 2011)

Supplementary Table S2 A summary of gene mutations in cells used in this study

cell	CRLF2-fusion	CRLF2 mutation	JAK mutation	RAS mutation	IKZF1 mutation	IKZF loss	CDKN2A/2B loss	TP53 mutation
MHH-CALL-4	*IGH@-CRLF2*		JAK2 I682F	KRAS L23R		Y	Y(homozygous)	N
MUTZ-5	*IGH@-CRLF2*		JAK2 R683G		IKZF1 M133fs	Y	Y(homozygous)	N
YCUB5	*CRLF2-P2RY8*		JAK2 R683I	KRAS G12D		Y	Y(homozygous)	N
NAGL-1	*IGH@-CRLF2*	CRLF2 F120C, F232C			IKZF1 L112fs		Y(homozygous)	N
KOPN49	*IGH@-CRLF2*		JAK2 R683G	KRAS G13D				R282fs (VAF=0.99)
case1	*IGH@-CRLF2*		JAK1 A634D		IKZF1 V110fs		Y(homozygous)	N
case2	*CRLF2-P2RY8*							N

Y: detected, N: not detected

Mutations in KOPN49 are according to the report by K. Sasaki, et al. (Blood, 2022;139(5):748-760). TP53 R282fs frame-shift mutation is a cancer hotspot (https://tp53.isb-cgc.org/results_somatic_mutation_list) and results in premature truncation of the functional protein. Due to the disruption of the DNA-binding domain and loss of the tetramerization domain (Genes Dev. 2012;26(12):1268-1286), R282fs is predicted to lead to a loss of Tp53 protein function (https://ckb.jax.org/geneVariant/show?geneVariantId=4742).

Supplementary methods

RNA extraction and transcript quantification

RNA isolated using the RNeasy Plus Micro Kit (Qiagen, Valencia, CA, USA) was reverse-transcribed using a High Capacity cDNA Reverse Transcription kit (Applied Biosystems, Waltham, MA, USA). The quantitative polymerase chain reaction analysis was performed using KOD FxNeo (Toyobo, Osaka, Japan) with SYBR Green. Reactions were run on the StepOnePlus Real-Time PCR System (Applied Biosystems).

Gene expression analysis

The cDNA library construction using NEBNextUltra RNA Library Prep Kit for Illumina (New England Biolabs, Ipswich, MA) and pair-end sequencing on the NovaSeq6000 platform (Illumina Inc., San Diego, CA) were performed by GeneNex/Chemical Dojin (Kumamoto, Japan). The paired-end reads were quality-filtered using Trim Galore and aligned to the hg19 human genome assembly using HISAT2 (v2.2.0). The expression level of each gene was calculated from the mapped reads using StringTie. Read counts obtained using prepDE.py were used for the analysis with the DESeq2 package (1.16.1) implemented in the R statistical software platform (version 4.0.5). Data were normalized with a variance-stabilizing transformation. The differential expression analysis was performed using DESeq2 (1). We selected genes with adjusted p-values of < 0.1 and fold-change values of > 1.5 for Metascape pathway analysis (2). GSVA analysis (3) was performed using R packages GSVA (version 1.38.1) and GSEABase (version 1.52.1) in combination with MSigDB hallmark gene sets (v7.2) provided by the Broad Institute. Changes in pathway activities were estimated using the R package PROGENy (version 1.14.0) (4). Scatter plots and heatmaps were generated using the R packages ggplot2 (version 3.2.2) and pheatmap (version 1.0.12), respectively.

Target capture DNA sequencing

Target capture DNA sequencing was performed using the capture panel with 110 genes and 1484 single nucleotide polymorphism baits to detect single nucleotide variants, indels, and copy number variations, as described previously (5).

Plasmids

MSCV-*IL7R-IRES-hCD4*, MSCV-*P2RY8-CRLF2-IRES-eGFP*, MSCV-*Jak2 R683G-IRES-luc*, and MSCV-*Jak2 P933R -IRES-luc* were kindly provided by CG Mullighan (St. Jude Children's Research Hospital) (6). cDNAs for the *Jak2 R683G* and *Jak2*

P933R were cloned into the MSCV-*PGK-tNGFR* vector for use in this study. In addition, *STAT5B1*6* cDNA (an active form of STAT5B) (7) kindly provided by Toshio Kitamura (The University of Tokyo, Japan) was cloned into the CSII-EF-*ires-PuroR* vector for amphotropic lentivirus production. CSII-hU6-PGK-hCD8 was used for shRNA.

Flow cytometric and western blot analyses

Flow cytometric analysis was performed using an LSRFortessa X-20 (BD Bioscience, Franklin Lakes, NJ). Antibodies used for flow cytometry and western blot are listed in Supplementary Table 1.

Analysis of mitochondrial membrane potentials

Mitochondrial membrane potential was measured using JC-1 according to the manufacturer's instructions. Briefly, cells were treated with ruxolitinib, FX1, or their combination for 24 hr and incubated with JC-1 (2 μM) for an additional 30 min. Fluorescence was measured on SpectraMax M5 plate reader (Molecular Devices, San Jose, CA) with excitation/emission wavelengths of 485 nm/530 nm and 535 nm/600nm.

Clinical information

Case 1 is a 24-year-old male with an initial peripheral white blood cell count of 5400/μl and 47, XY, +5[7], /46, XY karyotype, and received bone marrow transplantation after relapse. Case 2 is a 12-year-old man with an initial peripheral white blood cell count of 3900/μl and normal karyotype and received bone marrow transplantation after relapse.

References

1. Love MI, Huber W, Anders S. Moderated estimation of fold change and dispersion for RNA-seq data with DESeq2. Genome Biol. 2014;15(12):550.
2. Zhou Y, Zhou B, Pache L, Chang M, Khodabakhshi AH, Tanaseichuk O, et al. Metascape provides a biologist-oriented resource for the analysis of systems-level datasets. Nat Commun. 2019;10(1):1523.
3. Hänzelmann S, Castelo R, Guinney J. GSVA: gene set variation analysis for microarray and RNA-seq data. BMC Bioinformatics. 2013;14,7.
4. Schubert M, Klinger B, Klunemann M, Sieber A, Uhlitz F, Sauer S, et al. Perturbation-response genes reveal signaling footprints in cancer gene expression. Nat Commun. 2018;9(1):20.

5. Yasuda T, Sanada M, Kawazu M, Kojima S, Tsuzuki S, Ueno H, et al. Two novel high-risk adult B-cell acute lymphoblastic leukemia subtypes with high expression of CDX2 and IDH1/2 mutations. Blood. 2022;139(12):1850-1862.
6. Mullighan CG, Collins-Underwood JR, Phillips LA, Loudin MG, Liu W, Zhang J, et al. Rearrangement of CRLF2 in B-progenitor- and Down syndrome-associated acute lymphoblastic leukemia. Nat Genet. 2009;41(11):1243-1246.
7. Onishi M, Nosaka T, Misawa K, Mui AL-F, Gorman D, McMahon M, et al. Identification and characterization of a constitutively active STAT5 mutant that promotes cell proliferation. Molecular and cellular biology. 1998;18(7):3871-3879.

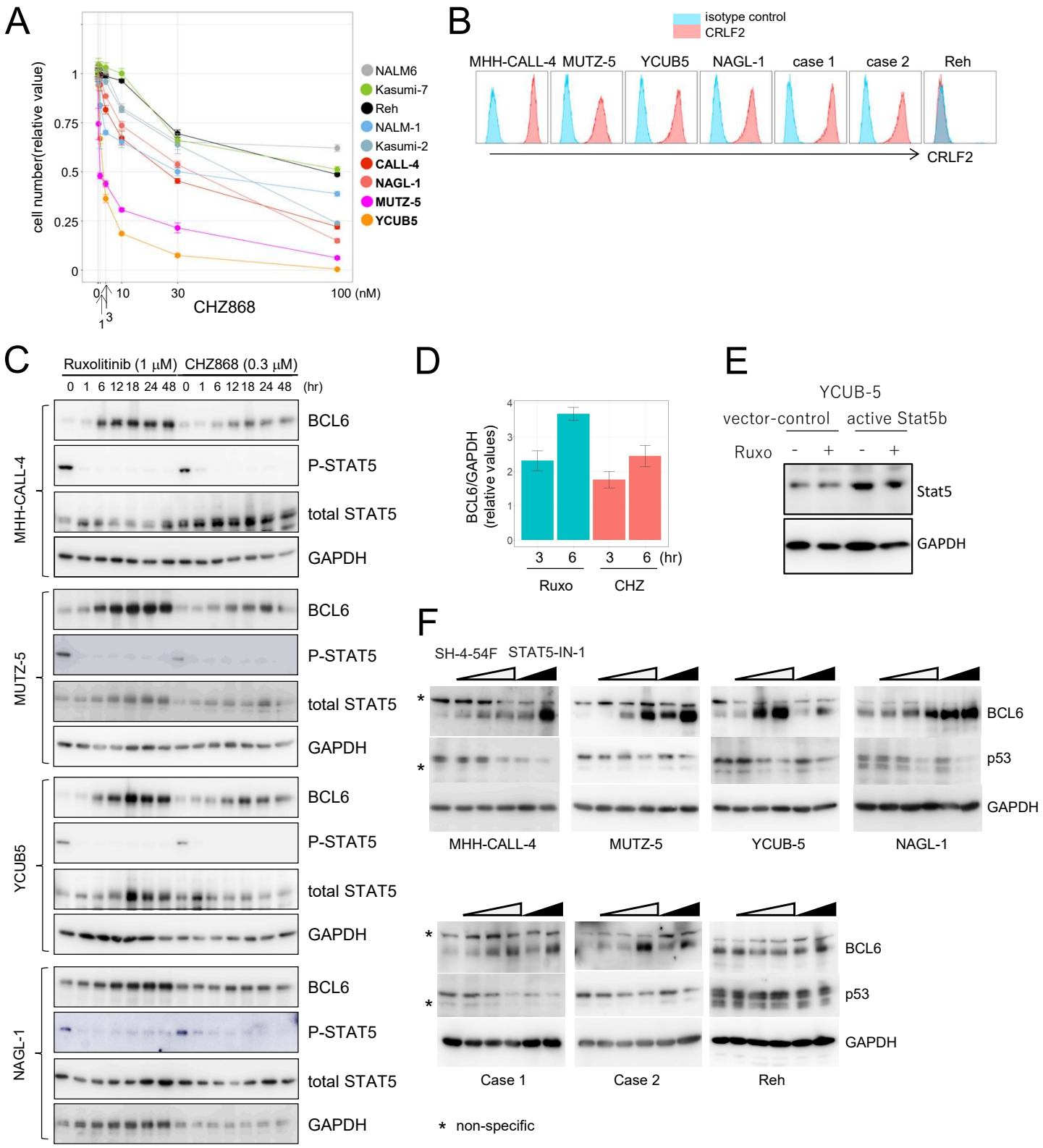

Figure S1

Growth inhibition by CHZ868, CRLF2 expression on cells, and BCL6 upregulation by JAK and STAT5 inhibitors

(A) Cells were cultured with the indicated concentration of CHZ868 for five days, and the relative growth compared to vehicle-treated cells is represented as the mean ± SD. (B) Cell surface expression of CRLF2. The four indicated CRLF2-ALL cell lines and two CRLF2-ALL clinical samples were stained with anti-CRLF2 or control antibodies for flow-cytometric analysis. A non-CRLF2-ALL Reh cell line served as a negative control. (C) Four CRLF2-ALL cell lines were treated with ruxolitinib (1 μM) or CHZ868 (0.3 μM). The expression of BCL6, phospho-STAT5, and total STAT-5 after the indicated treatment period was analyzed by western blot. The GAPDH served as a loading control. (D) The MHH-CALL-4 cells were treated with ruxolitinib or CHZ868 for 3h and 6 h, and quantitative RT-PCR determined BCL6 transcript levels. Normalized values based on GAPDH transcript levels are represented as fold-changes (mean ± SD) compared with the vehicle-treated cells. (E) Western blot analysis demonstrates the successful expression of an active form of STAT5B. An antibody reactive to both human and mouse STAT5s was used, with GAPDH as a loading control. (F) Western blot analysis showing the effects of a STAT3/5 inhibitor (SH-4-54F) and a STAT5 inhibitor (STAT5-IN-1) on BCL6, TP53, and GAPDH (loading control) expression. Asterisks show nonspecific bands.

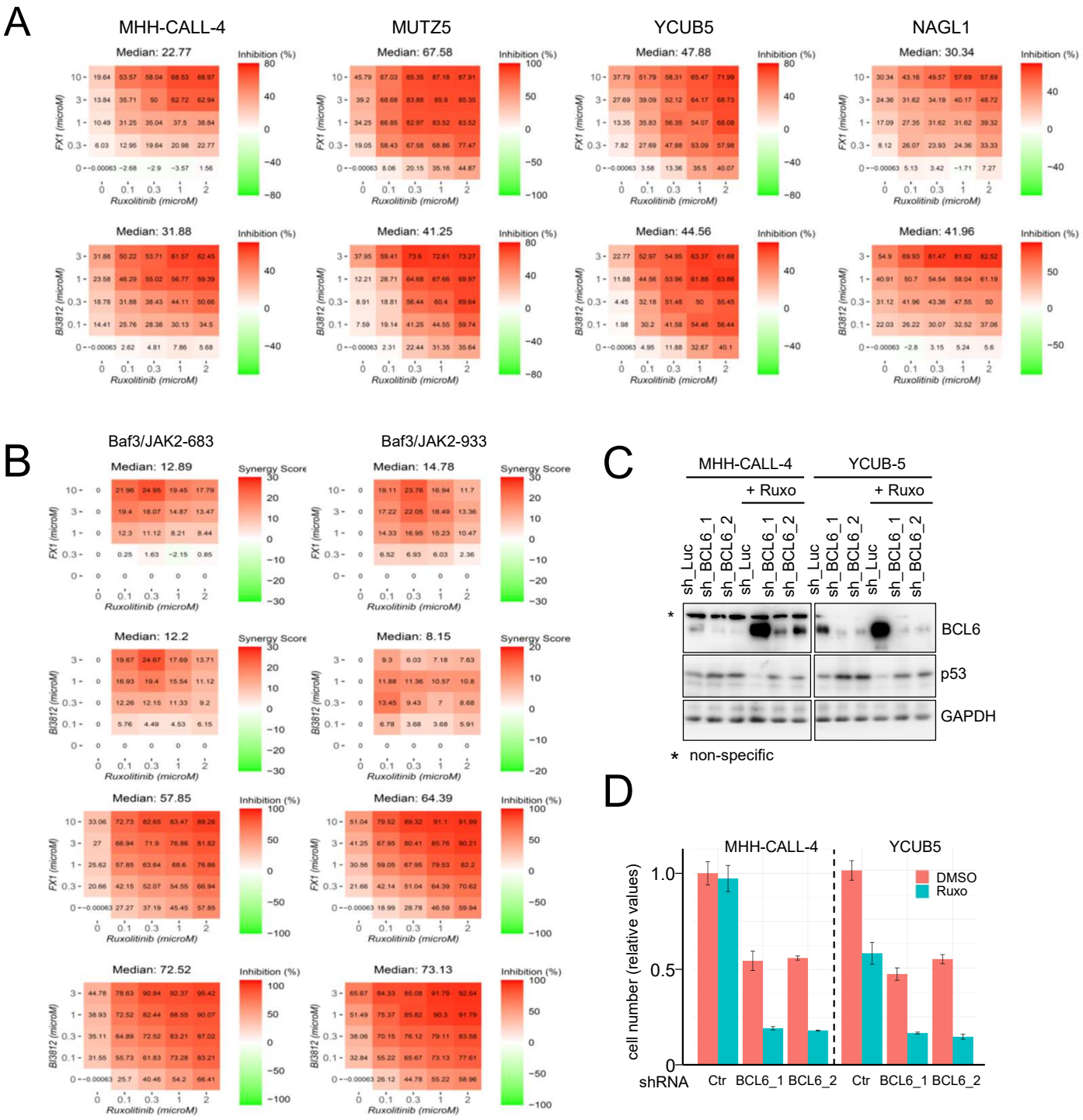
A
MHH-CALL-4
MUTZ5
YCUB5
NAGL1
Median: 22.77
Median: 67.58
Median: 47.88
Median: 30.34
Median: 31.88
Median: 41.25
Median: 44.56
Median: 41.96
Inhibition (%)
FX1 (microM)
BI3812 (microM)
Ruxolitinib (microM)
B
Baf3/JAK2-683
Baf3/JAK2-933
Median: 12.89
Median: 14.78
Median: 12.2
Median: 8.15
Median: 57.85
Median: 64.39
Median: 72.52
Median: 73.13
Synergy Score
C
MHH-CALL-4
YCUB-5
+ Ruxo
sh_Luc
sh_BCL6_1
sh_BCL6_2
BCL6
p53
GAPDH
* non-specific
D
MHH-CALL-4
YCUB5
DMSO
Ruxo
cell number (relative values)
shRNA
Ctr
BCL6_1
BCL6_2

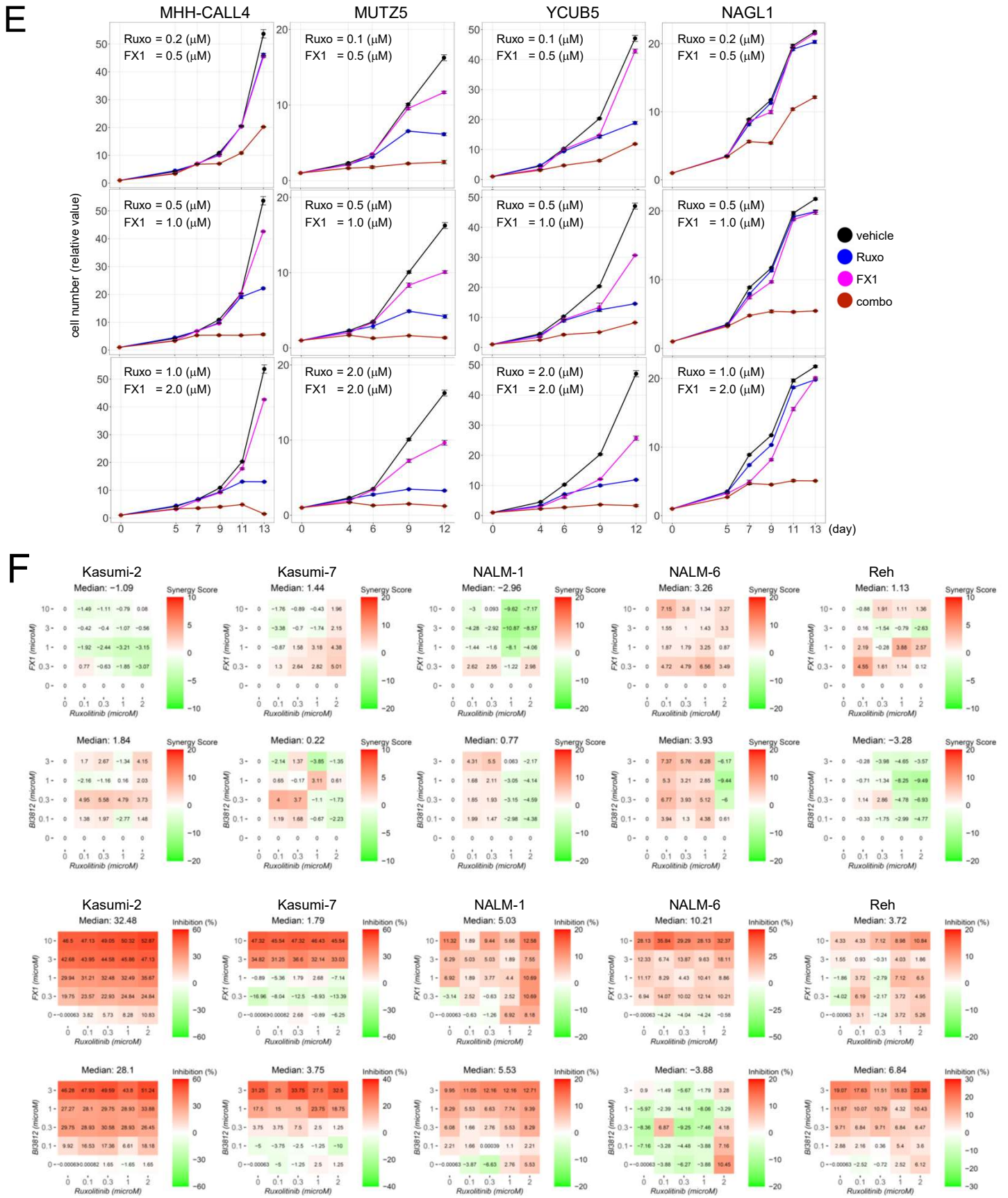

Figure S2

The synergy between ruxolitinib and BCL6 inhibitors for growth inhibition; and the effects of BCL6 knockdown

(A) Percent growth inhibition of cells shown in Figure 2. (B) Baf3 cells transformed by the enforced expression of CRLF2, IL7R, and JAK2 R683G or JAK2 P933R were treated as in Figure 2. The ZIP synergy scores (upper panels) and percent growth inhibition (lower panels). (C) Two CRLF2-ALL cell lines were infected with distinct lentiviruses for BCL6 knockdown. Cells were treated with ruxolitinib (1 μM) or DMSO for 24 h, and BCL6, p53, and GAPDH expression was analyzed by western blot. The shRNA for luciferase served as a control. (D) The growth of the indicated cells infected with shRNA for BCL6 (BCL6_1, BCL6_2) or luciferase (Ctr: control) in the presence of ruxolitinib or DMSO (control). Data are presented as relative cell numbers compared to DMSO-treated, control shRNA-infected cells. (E) Time-course analysis of cell growth. The CRLF2-ALL cells were treated with the indicated concentrations of ruxolitinib, FX1, and their combination. Cell growth was monitored for up to 13 days, and cell numbers are shown as the relative values (mean ± SD) to day 0. (F) Five non-CRLF2-ALL cells were treated as in Figure 2. The ZIP synergy scores (upper panels) and percent growth inhibition (lower panels) are presented.

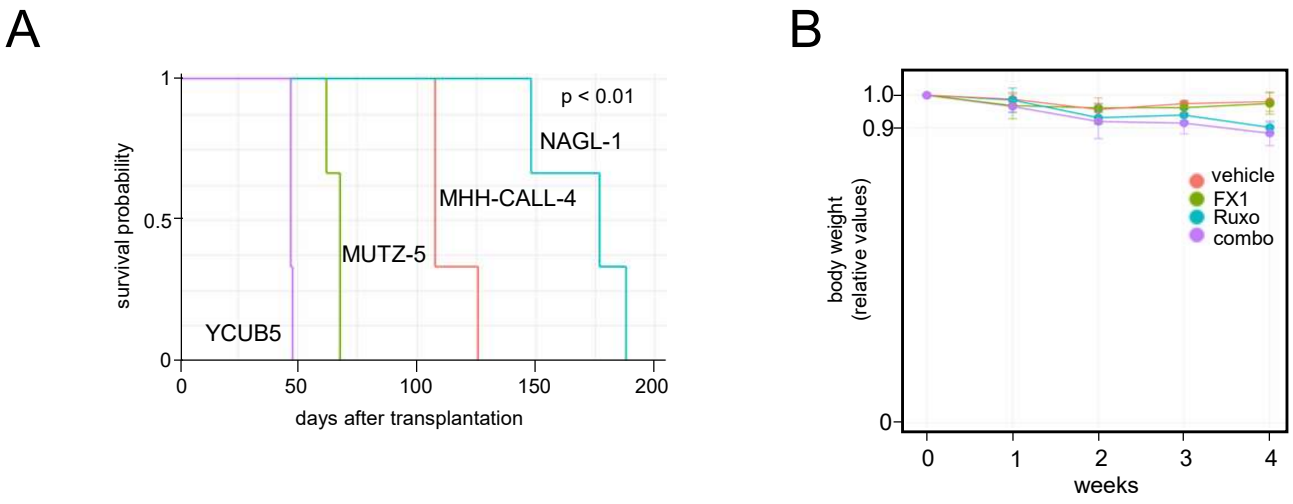

Figure S3

Survival and body weight change of NSG mice

(A) Immune-deficient NSG mice (n = 3 each) were implanted with an equal number of the indicated CRLF2-ALL cells and monitored for survival. The difference in survival was statistically significant ($p < 0.01$ by the log-rank test). (B) Bodyweight changes of mice used in Figure 3C. Bodyweight before the experiment was set to 1, and relative values ± SD are shown.

A

p53 PATHWAY

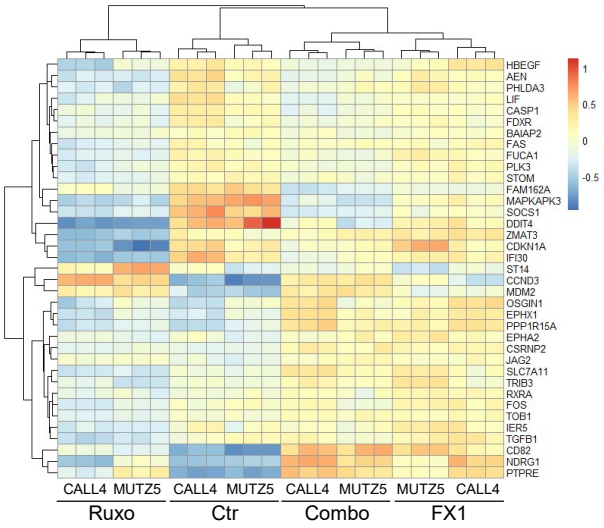

apoptosis signaling pathway

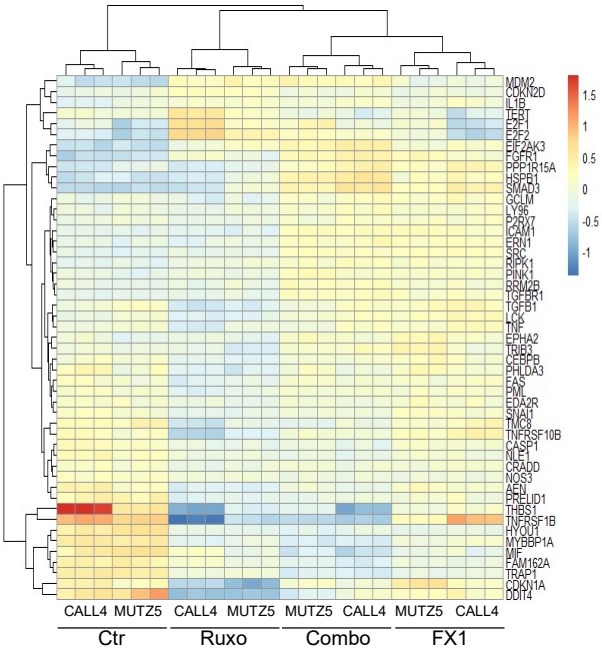

IL2-STAT5 SIGNALING

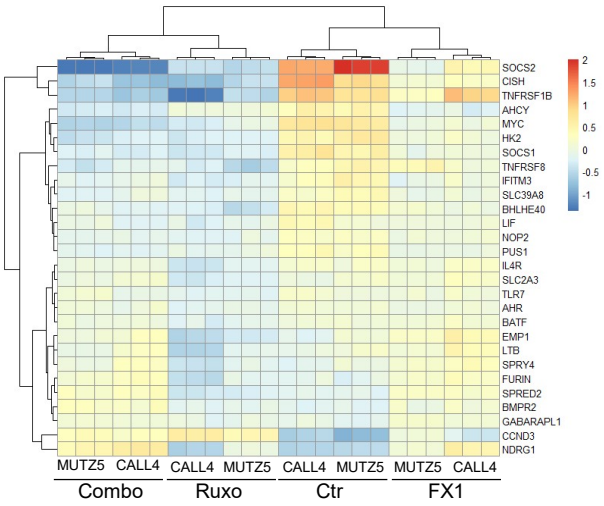

MYC_TARGETS_V2

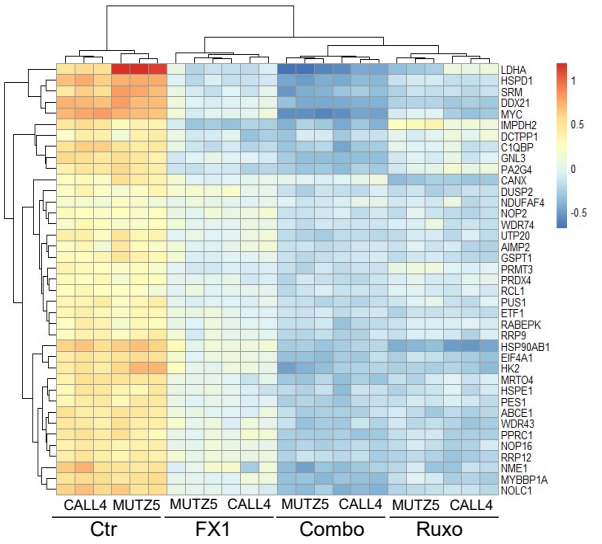

B

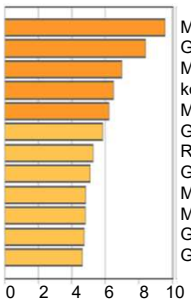

M5939: HALLMARK P53 PATHWAY
GO:0050865: regulation of cell activation
M145: PID P53 DOWNSTREAM PATHWAY
ko04520: Adherens junction
M19: PID P73 PATHWAY
GO:0042832: defense response to protozoan
R-HSA-202733: Cell surface interactions at the vesicular wall
GO:0002274: myeloid leukocyte activation
M5947: HALLMARK IL2 STAT5 SIGNALING
M5890: HALLMARK TNFA SIGNALING VIA NFKB
GO:0050866: negative regulation of cell activation
GO:1901654: response to ketone

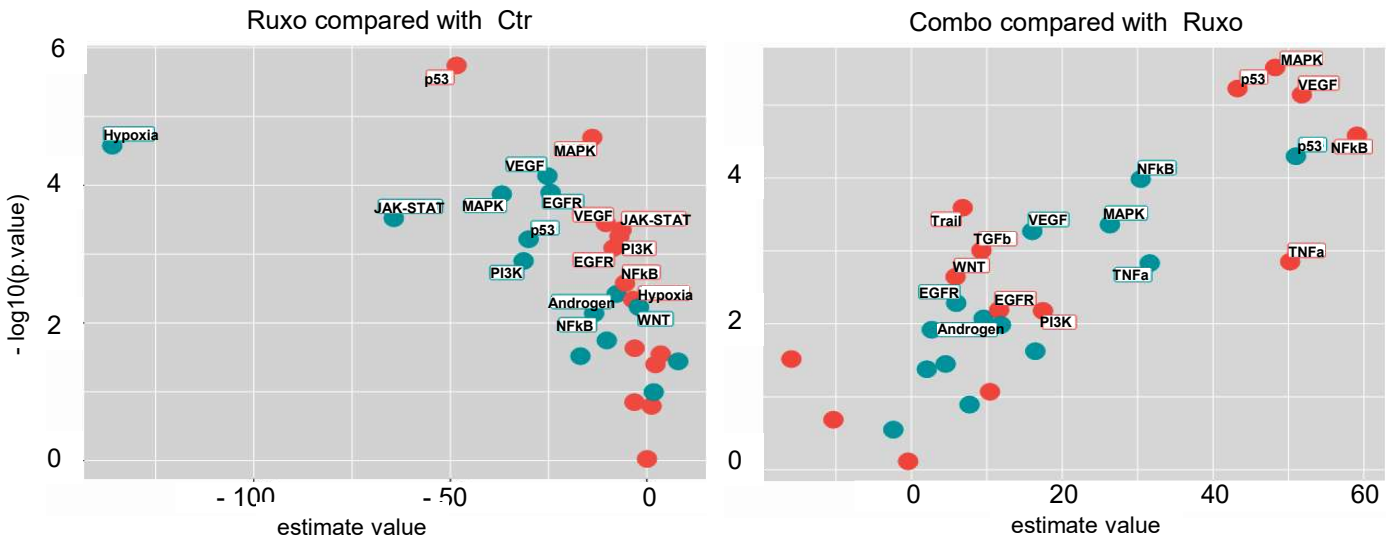

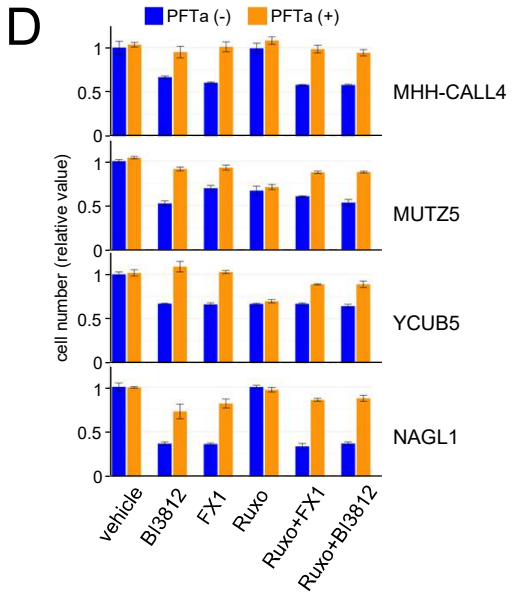

Figure S4

Gene expression changes by ruxolitinib and FX1

(A) The MHH-CALL-4 and MUTZ-5 cells were treated with ruxolitinib (Ruxo), FX1, and their combination (Combo), as in Figure 4A. Vehicle-treated cells served as a control. Heatmap representations of gene expression changes in the TP53-, apoptosis-, STAT5-pathways, and MYC target genes are provided. Genes commonly changed in both cells are selected. (B) Pathways enriched in genes that were downregulated by ruxolitinib, and again upregulated by ruxolitinib + FX1 compared to ruxolitinib alone. (C) PROGENy analysis of pathway activity. Horizontal and vertical axes show the degree of change in activity and $-\log_{10}(p\text{-value})$, respectively. Effects of ruxolitinib treatment compared to control (left) and effects of FX1 on ruxolitinib-treated cells (right) are shown, with red and green representing MHH-CALL-4 and MUTZ-5 cells, respectively. (D) Effects of a TP53 transcription activity inhibitor on cell growth. Four CRLF2-ALL cells were treated with the drugs, as indicated at the bottom, in the presence (orange) or absence (blue) of pifithrin-α (a TP53 inhibitor) for five days. Cell growth relative to vehicle-treated cells is shown as the mean ± SD.

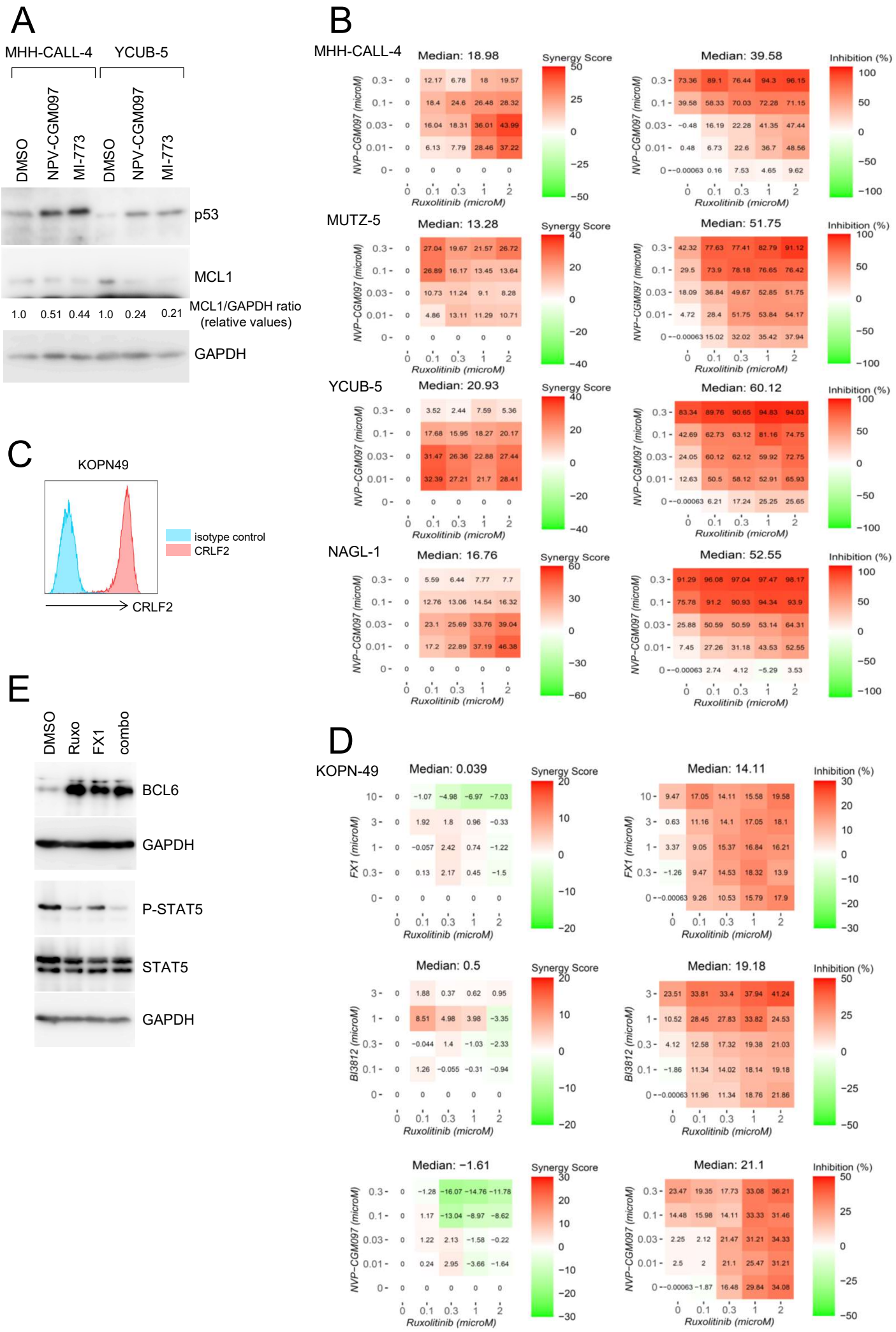
A
MHH-CALL-4
YCUB-5
DMSO
NPV-CGM097
MI-773
DMSO
NPV-CGM097
MI-773
p53
MCL1
1.0 0.51 0.44 1.0 0.24 0.21
MCL1/GAPDH ratio (relative values)
GAPDH
B
MHH-CALL-4
Median: 18.98
Median: 39.58
MUTZ-5
Median: 13.28
Median: 51.75
YCUB-5
Median: 20.93
Median: 60.12
NAGL-1
Median: 16.76
Median: 52.55
NVP-CGM097 (microM)
Ruxolitinib (microM)
Synergy Score
Inhibition (%)
C
KOPN49
isotype control
CRLF2
CRLF2
D
KOPN-49
Median: 0.039
Median: 14.11
Median: 0.5
Median: 19.18
Median: −1.61
Median: 21.1
FX1 (microM)
BI3812 (microM)
Ruxolitinib (microM)
Synergy Score
Inhibition (%)
E
DMSO
Ruxo
FX1
combo
BCL6
GAPDH
P-STAT5
STAT5
GAPDH

F

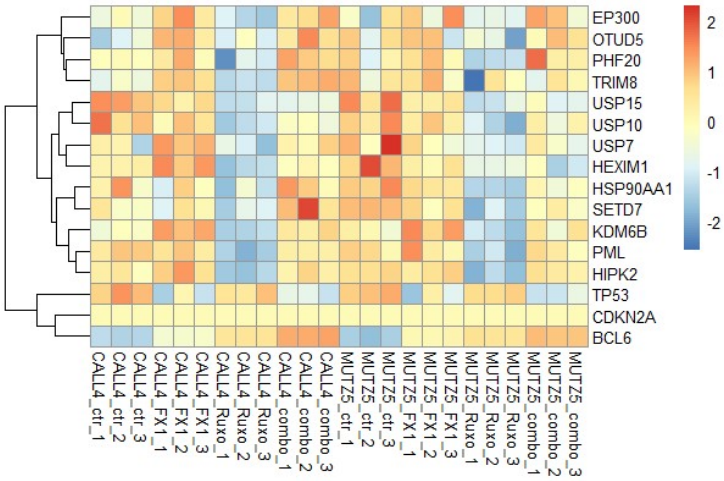
EP300
OTUD5
PHF20
TRIM8
USP15
USP10
USP7
HEXIM1
HSP90AA1
SETD7
KDM6B
PML
HIPK2
TP53
CDKN2A
BCL6
2
1
0
-1
-2
CALL4_ctr_1
CALL4_ctr_2
CALL4_ctr_3
CALL4_FX1_1
CALL4_FX1_2
CALL4_FX1_3
CALL4_Ruxo_1
CALL4_Ruxo_2
CALL4_Ruxo_3
CALL4_combo_1
CALL4_combo_2
CALL4_combo_3
MUTZ5_ctr_1
MUTZ5_ctr_2
MUTZ5_ctr_3
MUTZ5_FX1_1
MUTZ5_FX1_2
MUTZ5_FX1_3
MUTZ5_Ruxo_1
MUTZ5_Ruxo_2
MUTZ5_Ruxo_3
MUTZ5_combo_1
MUTZ5_combo_2
MUTZ5_combo_3

G

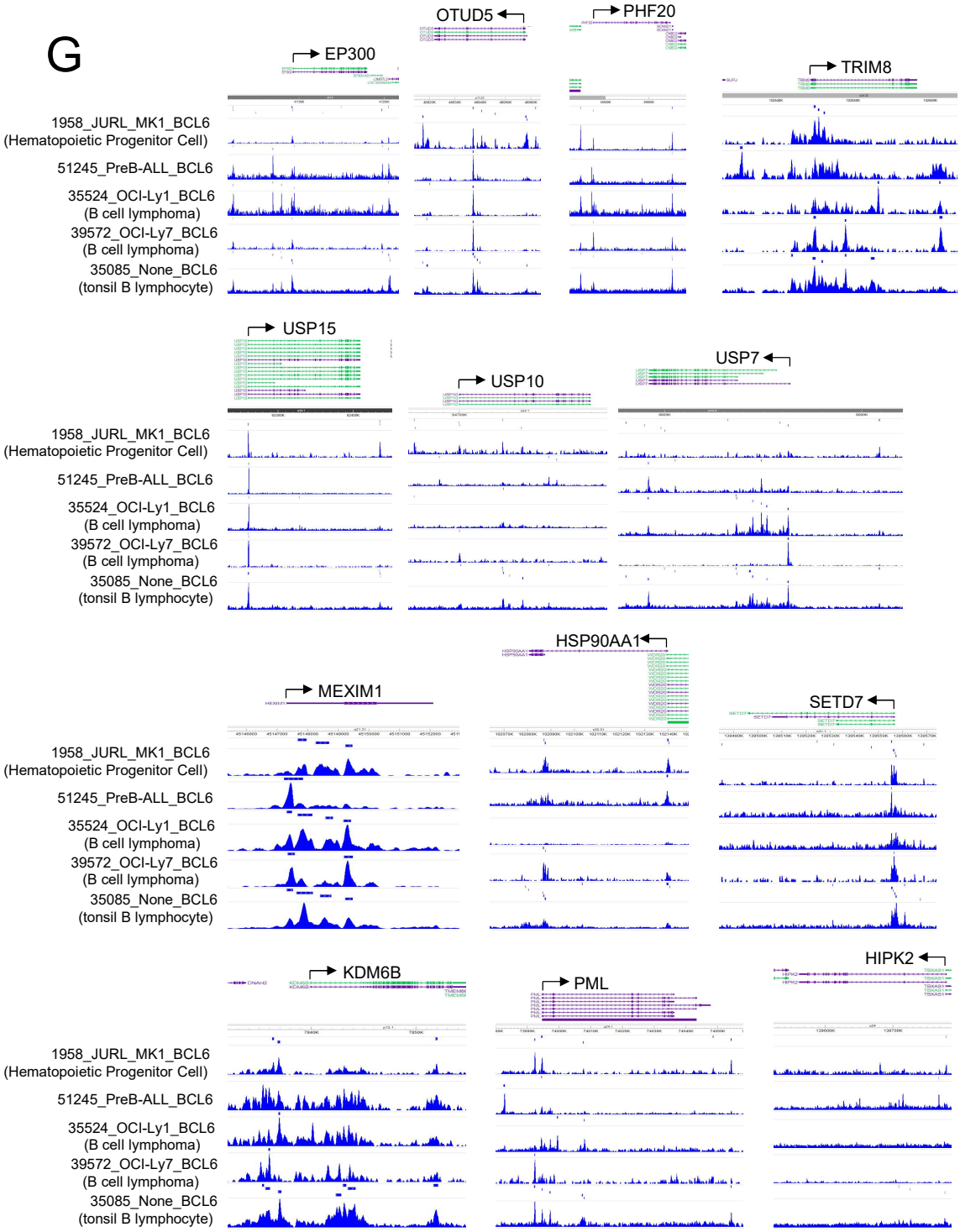
EP300
OTUD5
PHF20
TRIM8
USP15
USP10
USP7
HSP90AA1
MEXIM1
SETD7
KDM6B
PML
HIPK2
1958_JURL_MK1_BCL6
(Hematopoietic Progenitor Cell)
51245_PreB-ALL_BCL6
35524_OCI-Ly1_BCL6
(B cell lymphoma)
39572_OCI-Ly7_BCL6
(B cell lymphoma)
35085_None_BCL6
(tonsil B lymphocyte)

Figure S5

Effects of MDM2 inhibitors, analysis of a TP53-mutated CRLF2-ALL cell line (KOPN49), and gene expression changes of genes involved in TP53 protein stability

(A) Indicated CRLF2-ALL cells were treated with 0.3 μM of two MDM2 inhibitors (NVP-CGM097 and MI-773), and p53 and MCL1 expressions were analyzed along with GAPDH (loading control). (B) The ZIP synergy scores (left) and the percent inhibition of cell growth (right) of the indicated four CRLF2-ALL cells treated with the indicated concentrations of ruxolitinib and NVP-CGM097 in combination.

(C) Expression of CRLF2 on the surface of the KOPN49 cell line. (D) The ZIP synergy scores (left) and percent inhibition of cell growth (right) of KOPN49 cells treated with the combinations of the indicated concentrations of ruxolitinib and FX1, BI3812, or NVP-VGM097. (E) Upregulation of BCL in response to ruxolitinib and FX1 in KOPN49 cells. (F) A heatmap representation of changes in the expression of genes encoding molecules that stabilize the TP53 protein. (G) The BCL6 binding to the genomic regions near the transcription onset sites of the indicated genes. The BCL6 ChIP-seq data was made available by the Cistrome project and visualized on the Cistrome Data Browser (WashU version). Arrows indicate the direction of transcription. Prefix numbers indicate CistromeDB IDs.

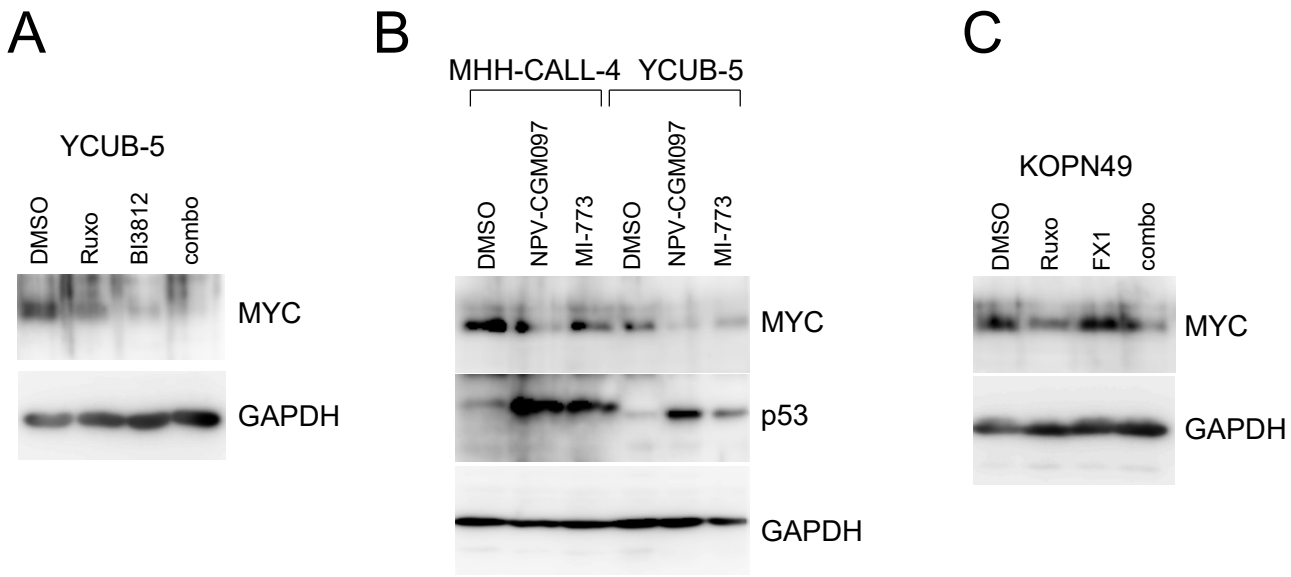

Figure S6
Analysis of MYC expression in CRLF2-ALL cells
(A) The YCUB-5 cells treated with ruxolitinib, BI3812, or their combination (as in Figure 5B) were analyzed for MYC expression by western blot.
(B) The MHH-CALL-4 and YCUB-5 cells treated with MDM2 inhibitors (NVP-CGM097 and MI-773) were analyzed for MYC and p53 expression by western blot. (C) The KOPN49 cells treated with ruxolitinib, FX1, and their combination, as in Figure 4A, were analyzed for MYC expression by western blot. The GAPDH served as loading controls in (A), (B), and (C).

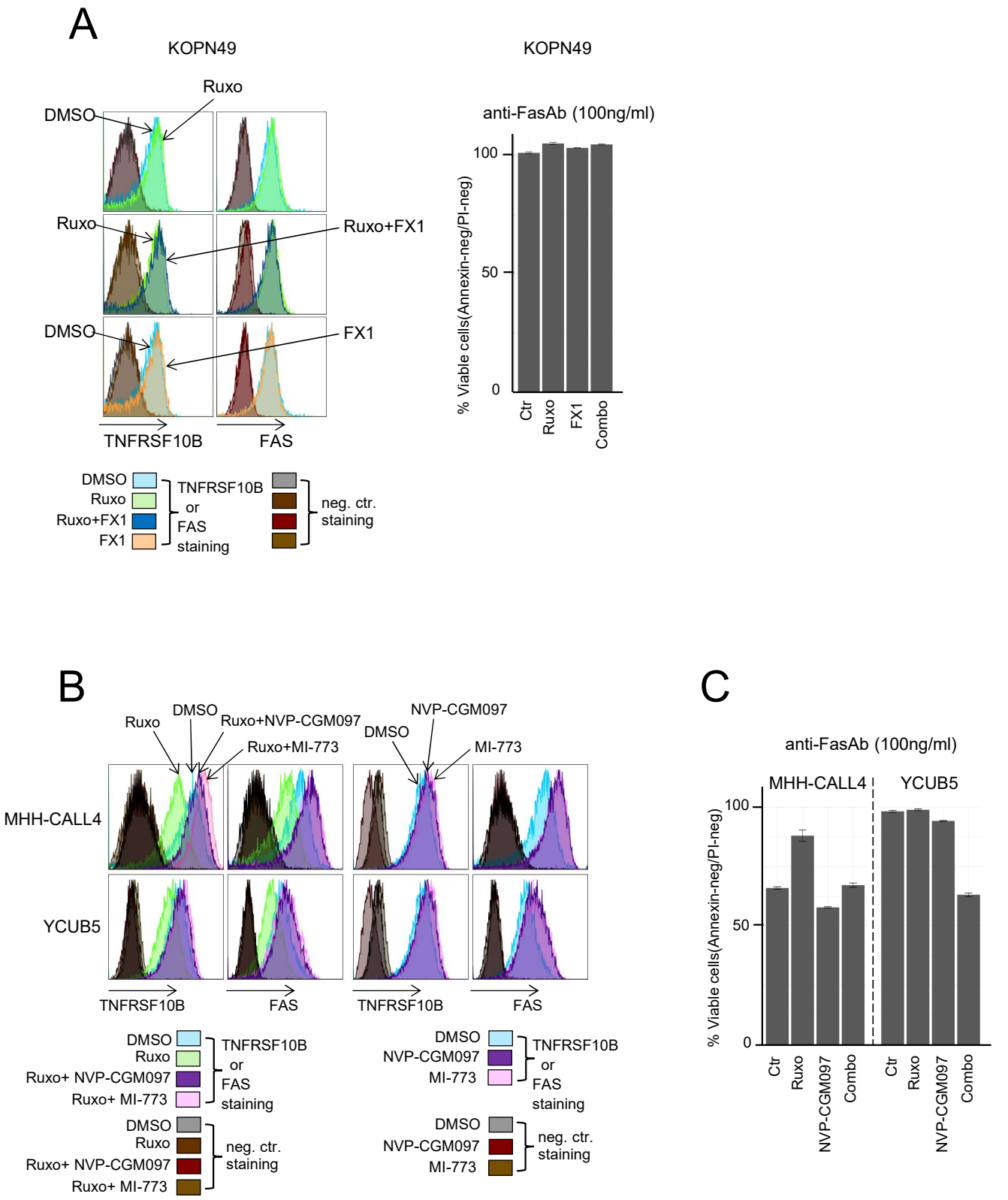

Figure S7

Analysis of extrinsic apoptosis pathways

(A) The KOPN49 cell line (TP53 biallelically mutated) was analyzed for TNFRSF10B and FAS expression after treatment with ruxolitinib, FX1, and their combination, by flow cytometry (left). Effects of anti-FAS antibody on cell viability (right). (B) Changes in TNFRSF10B and FAS expression on MHH-CALL-4 and YCUB-5 cells. Cells were treated with ruxolitinib or combinations of ruxolitinib with either NVP-CGM097 or MI-773 (left). Effects of NVP-CGM097 and MI-773 alone were analyzed (right). (C) Effects of ruxolitinib, NVP-CGM097, and their combination on FAS-mediated cell death. The viability of cells not treated with anti-FAS antibodies was normalized to 100%.

Figure S8

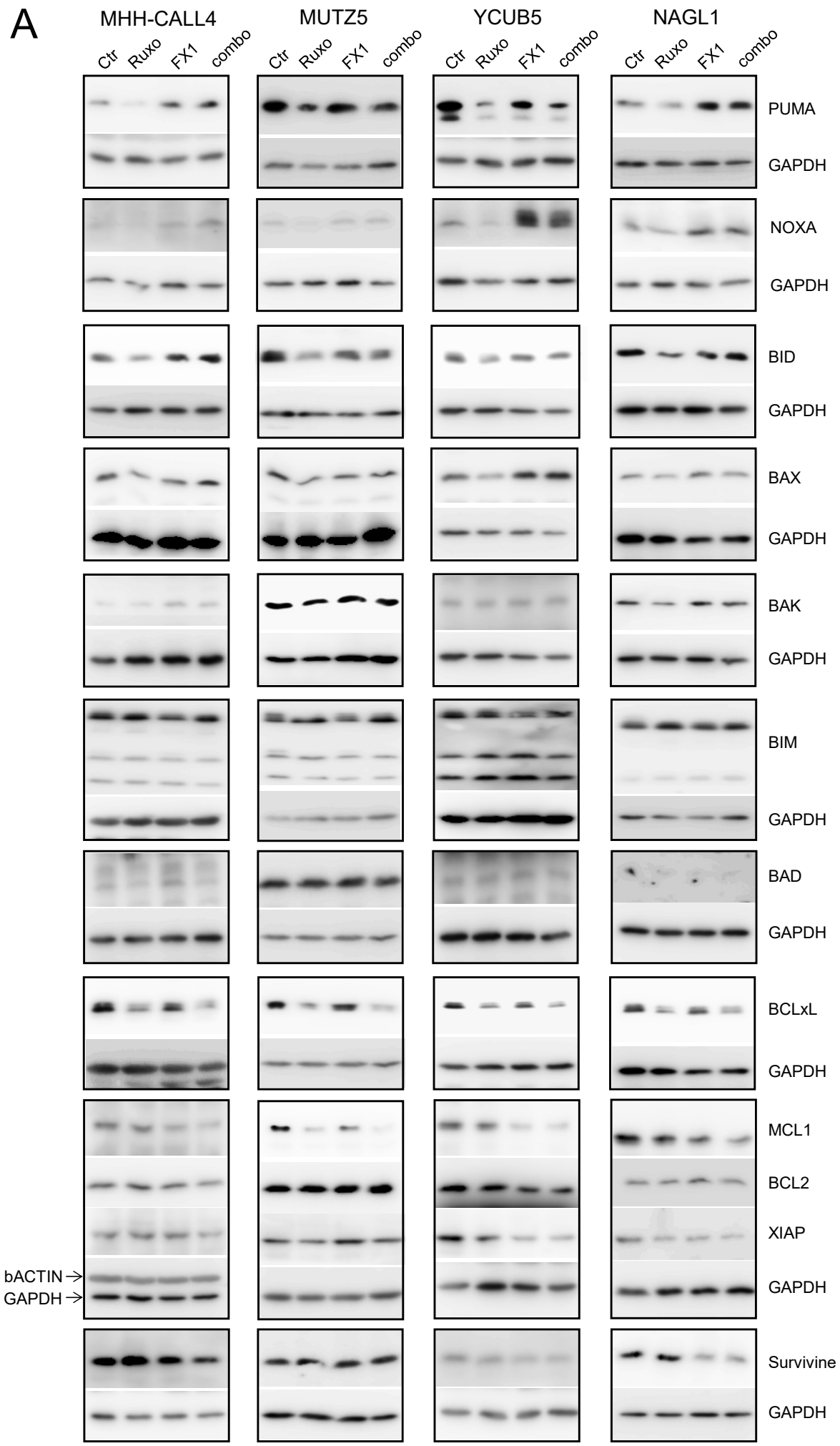
A
MHH-CALL4
MUTZ5
YCUB5
NAGL1
Ctr
Ruxo
FX1
combo
PUMA
GAPDH
NOXA
GAPDH
BID
GAPDH
BAX
GAPDH
BAK
GAPDH
BIM
GAPDH
BAD
GAPDH
BCLxL
GAPDH
MCL1
BCL2
XIAP
GAPDH
bACTIN
GAPDH
Survivine
GAPDH

Figure S8

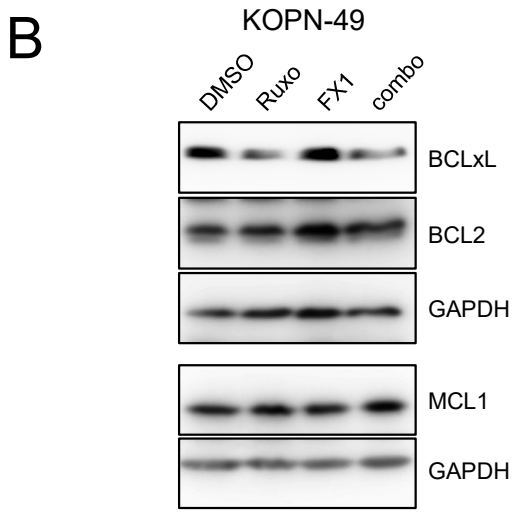
B
KOPN-49
DMSO
Ruxo
FX1
combo
BCLxL
BCL2
GAPDH
MCL1
GAPDH

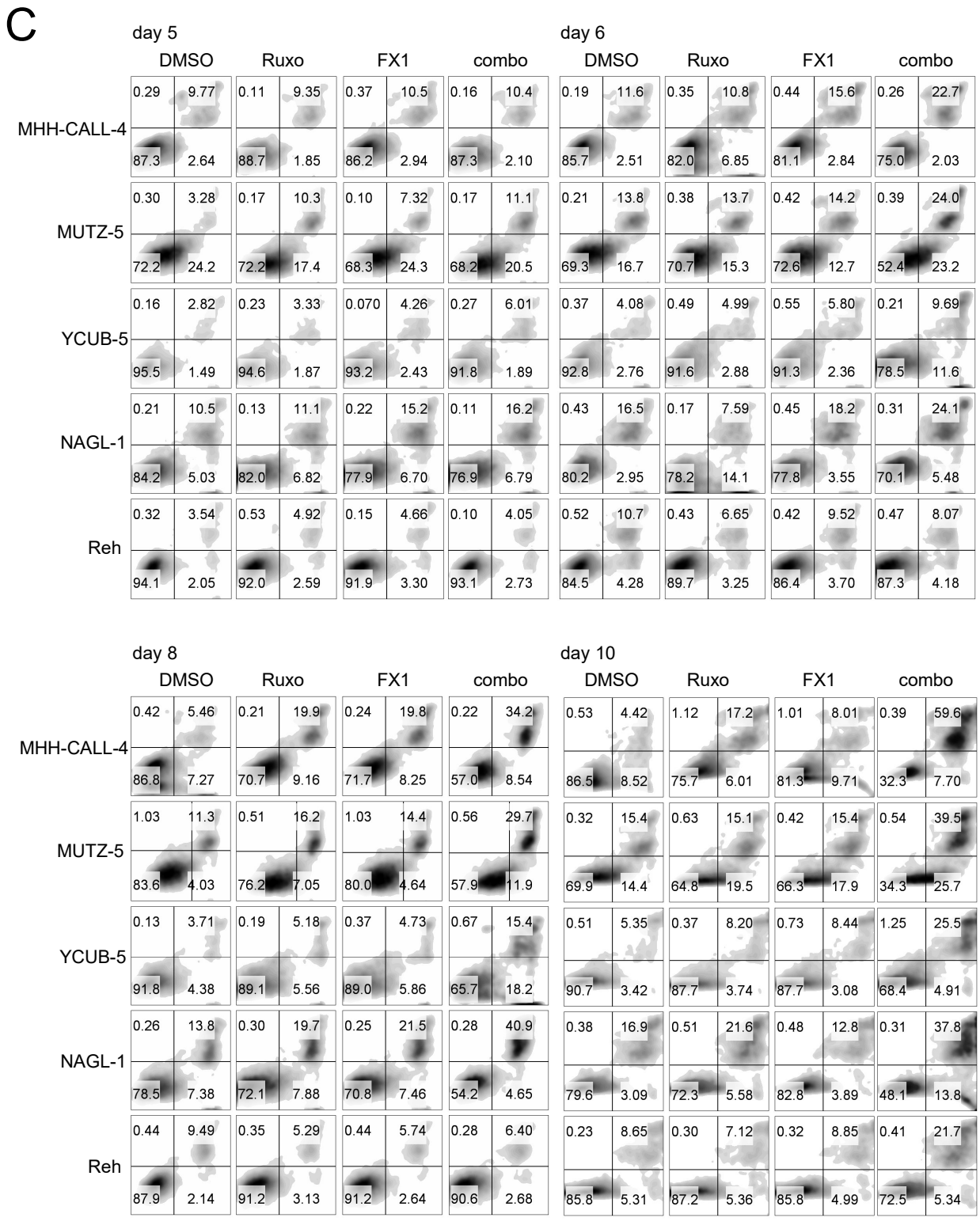
C
day 5
day 6
day 8
day 10
DMSO
Ruxo
FX1
combo
MHH-CALL-4
MUTZ-5
YCUB-5
NAGL-1
Reh

Figure S8

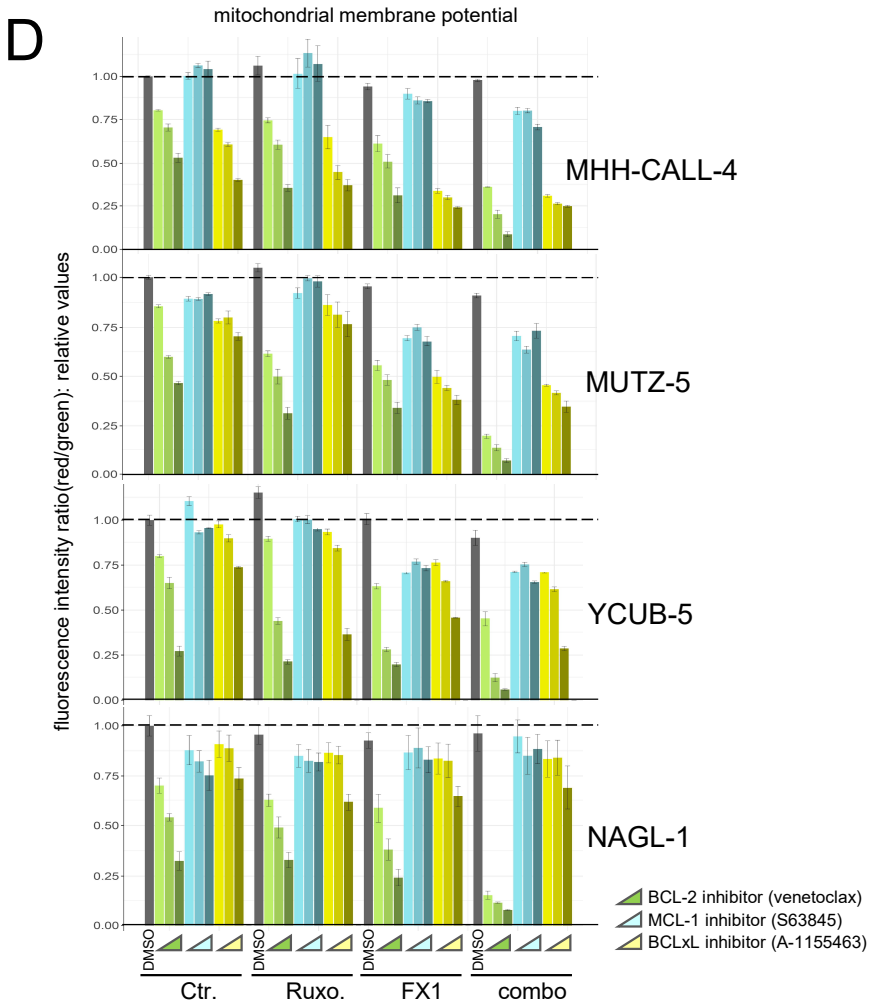
D
mitochondrial membrane potential
fluorescence intensity ratio(red/green): relative values
MHH-CALL-4
MUTZ-5
YCUB-5
NAGL-1
BCL-2 inhibitor (venetoclax)
MCL-1 inhibitor (S63845)
BCLxL inhibitor (A-1155463)
DMSO
Ctr.
Ruxo.
FX1
combo

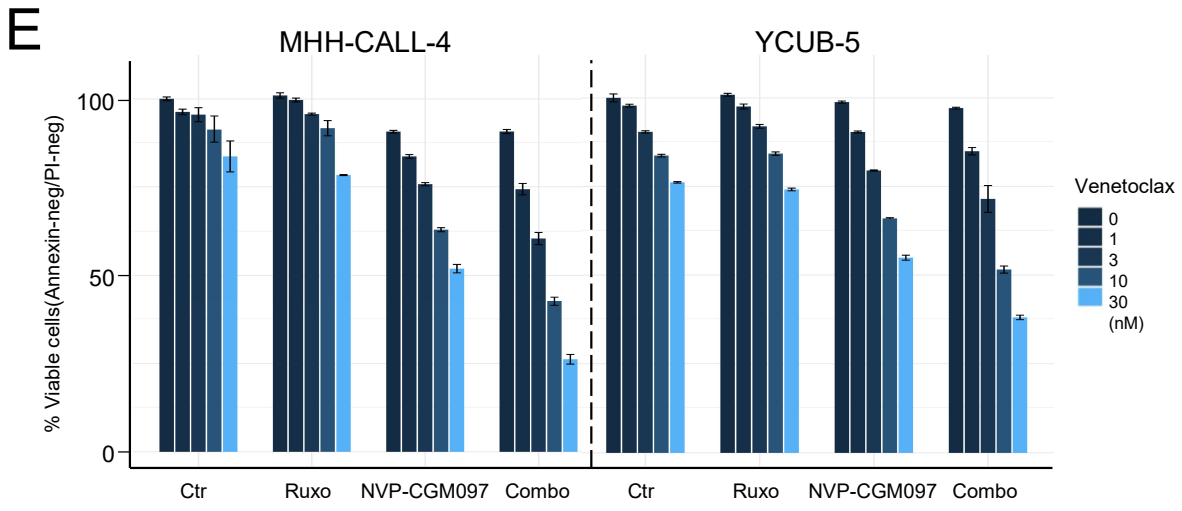
E
MHH-CALL-4
YCUB-5
% Viable cells(Annexin-neg/PI-neg)
Venetoclax
0
1
3
10
30
(nM)
Ctr
Ruxo
NVP-CGM097
Combo

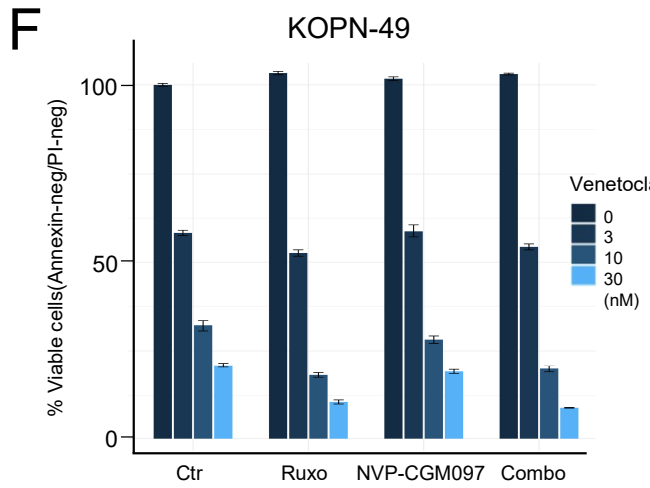
F
KOPN-49
% Viable cells(Annexin-neg/PI-neg)
Venetoclax
0
3
10
30
(nM)
Ctr
Ruxo
NVP-CGM097
Combo

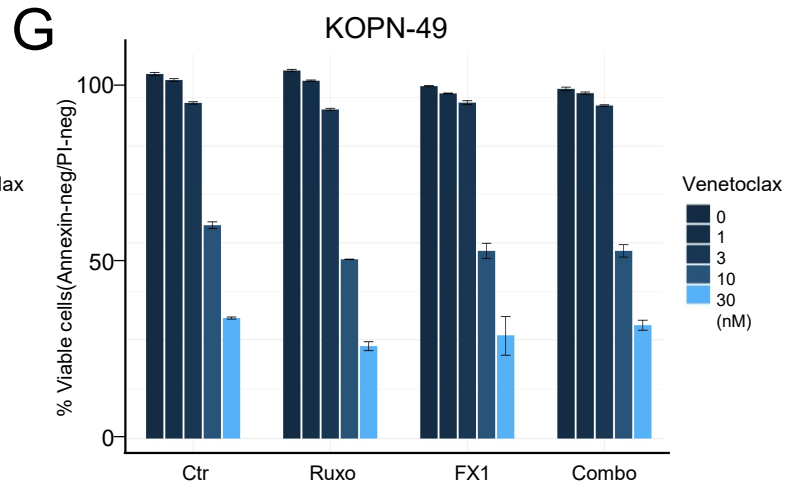
G
KOPN-49
% Viable cells(Annexin-neg/PI-neg)
Venetoclax
0
1
3
10
30
(nM)
Ctr
Ruxo
FX1
Combo

Figure S8

Analysis of intrinsic apoptosis pathways

(A) Four CRLF2-ALL cells were treated with ruxolitinib, FX1, and their combination for two days, and total cell lysates were analyzed for the expression of the indicated proteins. The GAPDH was used as a loading control. (B) The KOPN-49 cells were treated as indicated, and the expression of the indicated proteins was analyzed by western blot. (C) Four CRLF2-ALL cell lines were treated with ruxolitinib, FX1, their combination, and DMSO (vehicle) as in Figure 4A, and monitored for cell death by Annexin V/PI staining. Cell death was more prominent in the combination than in single-agent treatment, but only after six days of treatment. Reh, a non-CRLF2 ALL cell line, did not show such a tendency. (D) The mitochondrial membrane potential of cells. The four CRLF2-ALL cells were treated with DMSO (control: Ctr), ruxolitinib, FX1, and their combination for 24 hr and then treated with the graded concentrations of venetoclax (BCL2 inhibitor), S63845 (MCL-1 inhibitor), or A-1155463 (BCLxL inhibitor) for 4 hr, and the mitochondrial membrane potential was measured using JC-1. The mitochondrial potential of DMSO-only treated cells was set to 1.0, and relative values are presented. (E) The MHH-CALL-4 and YCUB-5 CRLF2-ALL cells were treated with ruxolitinib, NVP-CGM097 (an MDM2 inhibitor), and their combination, and then treated with the indicated graded concentrations of venetoclax, as in Figure 8C. The viabilities of cells are presented. (F, G) The KOPN-49 cells were treated with ruxolitinib, NVP-CGM097, their combination (F), ruxolitinib, FX1, or their combination (G), and then treated with the indicated graded concentrations of venetoclax. The relative viabilities of cells are presented.